Special Feature: Recent Research Developments on Periodic Mesoporous Organosilicas

Research Report

Excited-state Dynamics of Phenylene- and Biphenylylene-bridged Periodic Mesoporous Organosilica

Ken-ichi Yamanaka

∎**ABSTRACT**∥ In order to understand the excited-state dynamics of phenylene (Ph) and biphenylylene (Bp) moieties in the framework of periodic mesoporous organosilica (PMO), time-resolved fluorescence and absorption spectroscopic studies were carried out. The exciton fluorescence of Ph-PMO at room temperature was successfully analyzed using a one-dimensional diffusion model quenched by the defect center and the excimer site. The transient absorption spectra of Bp-PMO revealed intramolecular structural relaxation from the twisted Franck-Condon state to the lowest singlet excited state (S_1), and efficient quenching of the S_1 state by excimer formations. The differences between Ph-PMO and Bp-PMO were discussed.

∎**KEYWORDS**∥ Periodic Mesoporous Organosilica, Phenyl, Biphenyl, Excited State, Fluorescence, Transient Absorption

1. Introduction

Periodic mesoporous organosilicas (PMOs) are a new family of functional materials with organic-inorganic hybrid frameworks and well-defined mesochannels.[1-5] Various functionalities can be designed by the selection of organic groups incorporated in the framework.[6-10] Since the bridging organic groups are densely arranged, PMOs show unique photophysical and photochemical properties based on their intermolecular interactions such as efficient fluorescence emission,[11-15] light harvesting antenna,[16-19] photoinduced electron transfer,[20,21] and photoinduced hole transportation.[22] However, there have been few reports on the excited state dynamics of organic moieties in the framework of PMO although they are important to understand the mechanism of the unique photophysical and photochemical properties.

Time-resolved fluorescence and absorption spectroscopies are powerful tools to study the excited-state dynamics of materials. In the recent decade, we have investigated the excited-state dynamics of phenylene (Ph)-bridged PMO (Ph-PMO) and biphenylylene (Bp)-bridged PMO (Bp-PMO) by time-resolved spectroscopy.[20,23-28] Interestingly, Ph-PMO and Bp-PMO showed quite different excited-state dynamics although Ph and Bp have similar chemical structures. Here, we report the excited-state dynamics of Ph-PMO and Bp-PMO, and then discuss the difference in the dynamics between them.

2. Experimental

2. 1 Materials

Ph-PMO powder and its precursor molecule (1,4-bis(triethoxysilyl)benzene, BTEB) were prepared according to a previous report.[6] Ph-PMO consists of a Ph-silica hybrid framework and ordered mesochannels with a lattice constant a = 5.37 nm (2D-hexagonal), a pore diameter d_a = 4.09 nm, and a wall thickness $a - d_a$ = 1.28 nm (corresponding to the three Ph layers) as shown in **Fig. 1**(a). In the framework, the Ph moieties align perpendicular to the channel direction along the channels, forming a Ph-silica belt-like layer with an interval (d_i) of 0.76 nm. The Ph moieties are covalently fixed between the silicate layers, which hinders the close-packing of the Ph moieties. A molecular mechanics simulation showed that the neighboring Ph-Ph distance is approximately 0.44 nm, which is larger than the usual π-π stacking distance of aromatic compounds, although the molecular arrangement and intermolecular distance

can fluctuate due to the flexibility of the silicate layers and the existence of uncondensed silanol groups.

Bp-PMO powder was prepared by polycondensation of the organosilane precursor, 1,4-bis(triethoxysilyl)biphenyl (BTEBp), in the presence of a template surfactant, according to a previously reported method.[7] Bp-PMO powder consists of primary particles of approximately 300-500 nm in size and has a two-dimensional hexagonal lattice with a lattice constant of $a = 5.4$ nm and a pore diameter of $d_a = 3.5$ nm (Fig. 1(b)). The pore wall thickness ($a − d_a$) was calculated to be 1.9 nm, which corresponds to four layers of the Bp groups. In the pore wall, the Bp group aligns its molecular axis parallel to the mesochannel direction to form alternating Bp-silica belt-like layers with an interval of 1.19 nm. The Bp-Bp distance in the layer was estimated to be 0.44 nm from molecular mechanics simulations.[6]

2. 2 Apparatus

Steady-state absorption and fluorescence spectra were measured using a commercially available

Fig. 1 Schematic image of (a) Ph-PMO and (b) Bp-PMO.

spectrometer. Fluorescence decay curves were measured by a time-correlated single photon counting (TCSPC) system (Becker & Hickel, SPC-730 Module) as described elsewhere.[23] The third-harmonic generation (THG, 266 nm) of a mode-locked Ti:sapphire oscillator (Coherent, Vitesse) was used as the excitation light. The observed decay curves were deconvoluted by a home-made program created based on that demonstrated in the literature.[23,29] The time profile of the exciting light pulse (< 40 ps FWHM) was used as the instrumental response function (IRF) for deconvolution of the fluorescence time profiles. Femtosecond time-resolved spectra were measured using a pump-probe technique (CDP, ExciPro) as described elsewhere.[23] The THG pulse of a regenerative amplifier (Coherent, Legend) was used as an excitation light. For diffuse reflectance spectra, transient absorption intensity was analyzed as percentage absorption, $\%Abs = (1 − R/R_0) \times 100$, where R and R_0 represent the intensity of the diffuse reflected light of the probe pulse with and without excitation, respectively. The observed decay curves were analyzed using commercially available software.

3. Results and Discussion

3. 1 Excited State Dynamics of Ph-PMO

Figure 2(a) shows the fluorescence excitation spectra of Ph-PMO dispersed in MeOH/EtOH and BTEB in MeOH/EtOH at room temperature (RT). The excitation spectrum of Ph-PMO shifts to lower energy by about 500 cm^{-1} compared to that of BTEB due to the excitonic interaction between the Ph moieties. The interacting Ph moieties are probably in the direction of the belt-like layers (Fig. 1(a)). The emission at 280-300 nm and the broad band at around 340 nm were assigned to fluorescence from the Ph exciton and the excimer, respectively.

Figure 2(b) shows the temperature dependence of the fluorescence spectra of Ph-PMO. The excimer fluorescence (340 nm) decreased with decreasing temperature. This spectral change can be explained by the excimer formation occurring less frequently whereas the fluorescence band of the Ph exciton is clearly detected. The fluorescence with a maximum at around 305 nm remained unchanged as the temperature ranged from 293 to 175 K, unlike the other bands at 290 and 295 nm, which were assigned to the vibronic
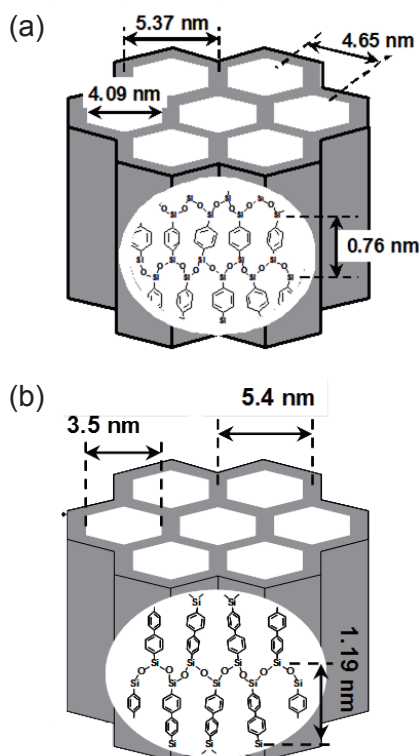
bands of the Ph moiety. The emission band at around 305 nm is attributed to the defect center of the silica framework, based on a report of efficient energy transfer from the S_1 state of benzene adsorbed on the surface of FSM-16 or SBA-15 to the photoactive defect center in the silica wall emitting at around 300 nm.[30]

Figure 2(c) shows the excitation spectra monitored at various emission wavelengths. Every excitation spectrum monitored at a different wavelength, including 305 nm, showed the same shape. This indicates that the excited state of the defect center for the emission at 305 nm originated from the exciton of Ph-PMO, and that dimers and/or aggregates of the Ph moieties were not formed in the ground state.

Figure 3 shows the time dependence of the fluorescence of Ph-PMO dispersed in MeOH/EtOH at RT. The fluorescence decay curve of the exciton observed at 290 nm showed a non-exponential time dependence (Fig. 3(a)), which indicates that the deactivation of the exciton state was apparently controlled by a process with a time-dependent reaction rate, $k(t)$. The time profile of the excimer fluorescence observed at 360 nm (Fig. 3(b)) showed a rise component at a short time region and decayed with a single exponential function at a longer time region, which indicates that one stable excimer state

Fig. 2 (a) Excitation and fluorescence spectra of Ph-PMO dispersed in MeOH/EtOH (solid line) and BTEB (0.44 mM) in MeOH/EtOH (dashed line) at RT. (b) Temperature dependence of the normalized fluorescence spectrum and (c) excitation spectra at 265 K and 79 K for Ph-PMO dispersed in MeOH/EtOH.
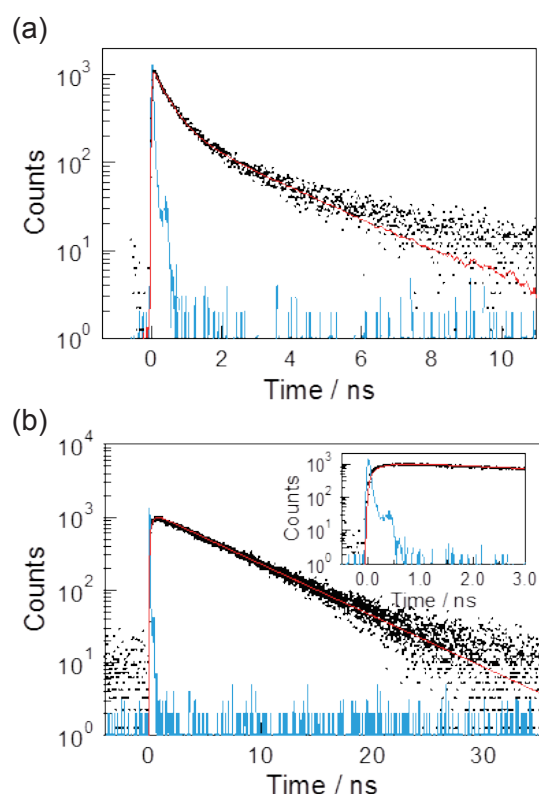
Fig. 3 Fluorescence decay curves of Ph-PMO dispersed in MeOH/EtOH detected at (a) 290 nm and (b) 360 nm. Inset in (b) shows short time region of the decay. Red and blue solid lines indicate the simulated result and IRF, respectively.

was formed from the exciton in Ph-PMO.

The time dependence of the fluorescence can be explained by the analytical model shown in **Scheme 1**, where Ph* is the exciton of the Ph moiety, Q is a quencher site of the defect center (C) or excimer site (E), $k(t)$ is the time-dependent quenching reaction rate of the exciton, and τ_{Ph}, τ_C, and τ_E are fluorescence lifetimes of the exciton, defect center, and excimer, respectively. Since the fluorescence property of Ph-PMO depends greatly on the temperature, processes without large molecular motion in the excited state such as Förster energy transfer are minor. Therefore, the energy transfer from the Ph exciton to the defect center and the excimer was excluded in this model. The time dependence of the Ph exciton and excimer is written by Eqs. (1) and (2) under the delta-function excitation condition,

$$dPh^*(t)/dt = -\tau_{Ph}^{-1} Ph^*(t) - c_0 k(t) Ph^*(t), \qquad (1)$$

$$dE^*(t)/dt = -\tau_E^{-1} E^*(t) + c_0 k(t) Ph^*(t), \qquad (2)$$

where $Ph^*(t)$ and $E^*(t)$ are densities of the Ph exciton and excimer, and c_0 is the one-dimensional quencher density ($c_0 = C + E^*$). When diffusion of the exciton is the rate-determining process, the $k(t)$ is written by Eq. (3),[31,32]

$$k(t) = (D/\pi t)^{1/2}, \qquad (3)$$
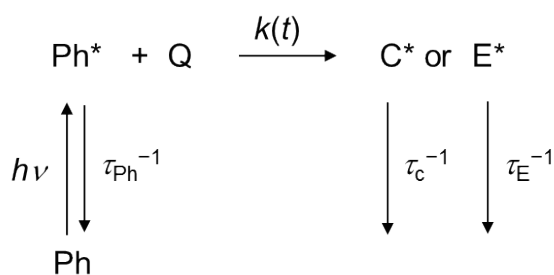
where D is the one-dimensional diffusion constant. By substituting Eq. (3) into Eqs. (1) and (2), we obtain the following equations:

$$Ph^*(t)/Ph_0 = \exp\{-t/\tau_{Ph} - 2c_0(Dt/\pi)^{1/2}\}, \qquad (4)$$

$$E^*(t) = Ph_0 c_0 (D/\pi)^{1/2} \exp(-t/\tau_E) \int_0^t t'^{-1/2}$$
$$\exp[(\tau_E^{-1} - \tau_{Ph}^{-1})t' - 2c_0(Dt'/\pi)^{1/2}]dt', \qquad (5)$$

where Ph_0 is the density of the Ph exciton at $t = 0$.

We analyzed the time dependence of the fluorescence at 290 nm by using Eq. (4). The decay curve observed at 290 nm includes the defect center decay as a minor component. Therefore, we used Eq. (6) for the analysis of the decay curve at 290 nm,

$$I_F(t)^{290\,nm} = A_1 Ph^*(t) + A_4 C^*(t)$$
$$= A_1 \exp(-t/A_2 - A_3 t^{1/2}) + A_4 \exp(-t/A_5), \qquad (6)$$

where A_n ($n = 1 - 5$) are fitting parameters. The best fitting result was obtained when $A_1 = 0.86$, $A_2 = 0.7$ ns, $A_3 = 4.5 \times 10^4$ s$^{-1/2}$, $A_4 = 0.14$, and $A_5 = 2.4$ ns, as shown in Fig. 3(a) (solid red line).

Next, time dependence of the excimer fluorescence was simulated by using Eq. (5). The values of $\tau_{Ph} = 0.7$ ns, $\tau_C = 2.4$ ns, and $2c_0(D/\pi)^{1/2} = 4.5 \times 10^4$ s$^{-1/2}$ ($c_0 D^{1/2} = 4 \times 10^4$ s$^{-1/2}$) obtained by Eqs. (4) and (6) were used. The lifetime of the excimer (τ_E) was evaluated to be 6.3 ns by the curve fitting with the single-exponential function in the time range from 2 to 40 ns. The integral in Eq. (5) was calculated numerically. In order to compare this simulation with the experimental results, the simulated $E^*(t)$ was convoluted by the instrumental response function (IRF) of the detection system. The convoluted $E^*(t)$ is shown in Fig. 3(b) (solid red line). This simulated result fairly reproduced the rise and decay of the excimer fluorescence, which indicates that the time dependence of the Ph-PMO fluorescence can be explained by this analytical model.

Although c_0 and D are unknown in the present study, some comments on the diffusion length $(\tau_{Ph}D)^{1/2}$ can be made based on the above results. The origin of photoluminescent defect centers in mesoporous silica materials has been investigated in relation to the surface silanols, including models involving interacting silanols[33,34] and reaction of the silanols with water molecules.[35] Carbonaro et al. assigned the photoluminescence band at 4.0 eV (310 nm) to a mutually H-bonded Si-OH pair.[33] Onida et al. carried

Ph* + Q $\xrightarrow{k(t)}$ C* or E*

$h\nu$ $\quad \tau_{Ph}^{-1}$ $\qquad\qquad \tau_C^{-1}$ $\quad \tau_E^{-1}$

Ph

Ph*: Exciton
Q: Quencher site of defect center (C) or excimer (E)
$k(t)$: Quenching reaction rate of exciton
τ_{Ph}, τ_C, and τ_E : Fluorescence lifetimes of the exciton, defect center and excimer, respectively.

Scheme 1　Reaction model of the excited state of Ph-PMO at RT.

out FTIR spectroscopy on silanols in crystal-like Ph-PMO and characterized them to be isolated silanols, mutually hydrogen bonded silanols and silanols interacting with a benzene ring.[36] In the present system of Ph-PMO, 16.5% of the Si-O bonds are uncondensed silanol groups, i.e., there is one silanol on average for one Ph moiety having six Si-O bonds. Thus, the concentrations of the Ph moieties and the silanols are calculated to be ca. 2.3×10^7 cm^{-1} using 0.44 nm for the Ph-Ph distance in the ideal model shown in Fig. 1(a). If we assume that 10% of the silanols forming H-bonded pairs are defect centers and 10% of the Ph moieties move their positions to form excimer sites, the diffusion length at 295 K is expected to be 2.3 nm, which corresponds to the exciton migration along five Ph moieties.

3. 2 Excited State Dynamics of Bp-PMO

Figure 4(a) shows fluorescence spectra of Bp-PMO dispersed in 2-methyltetrahydrofuran (2-MeTHF). Bp-PMO showed a structureless band with the maximum at 380 nm at 296 K. The band was red-shifted and broadened from that of BTEBp in cyclohexane, which showed peaks at 311 and 320 nm and a weak shoulder at 338 nm (solid line in Fig. 4(b)). The band of Bp-PMO was assigned to the Bp excimer bands reported for biphenyl in cyclodextrin oligomers and in a crystalline layered silicate.[37,38] The excimer fluorescence was also measured for BTEBp neat liquid (dashed line in Fig. 4(b)). At 77 K, the spectrum of Bp-PMO has peaks at 315, 327, and 340 nm and a broad band with a shoulder at 380 nm. Since the positions of the former three peaks were similar to those of BTEBp in cyclohexane, the observed spectrum of Bp-PMO at 77 K is well explained by a superposition of the monomer and excimer bands. Figure 4(c) shows the excitation spectra of Bp-PMO obtained at the monomer and excimer fluorescence wavelengths. No excitation wavelength dependence was found, which indicates that dimer or oligomer formation in the ground state is minor.

Figure 5(a) shows TDR spectra of Bp-PMO powder. A strong absorption band around 475 nm and a broad band centered at 680 nm were observed at 1 ps. At 2 ps, the intensity of the 475 nm band decreased by approximately 20% and the absorption was shifted to a shorter wavelength around 450 nm, whereas the broad band at 680 nm decayed only slightly. This

spectral change from 1 to 2 ps can be explained as a structural relaxation process from the twisted Franck-Condon (FC) state to the relaxed lowest singlet excited (S_1) state as described later. In the 2-10 ps time region, the 450 nm absorption band was significantly decayed by approximately 40% while maintaining its spectral shape. The band then decayed further, but more slowly, in the time period of 10-500 ps. These results indicate that fast (< 10 ps)
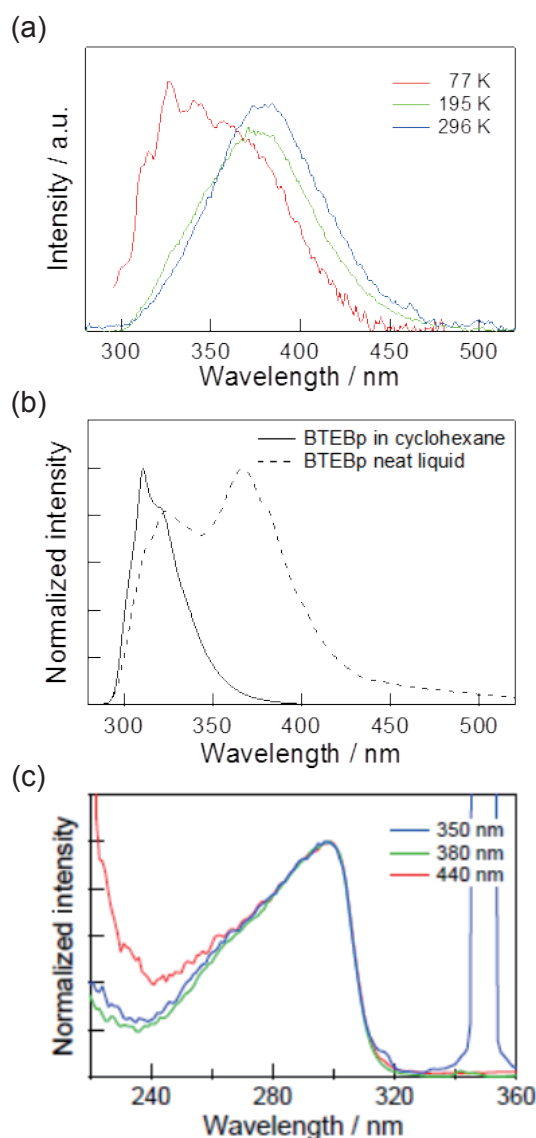
Fig. 4 (a) Temperature dependence of the fluorescence spectra of Bp-PMO dispersed in 2-MeTHF. (b) Fluorescence spectra of BTEBp in cyclohexane (0.3 mM) and the neat liquid at room temperature. (c) Fluorescence excitation spectra of Bp-PMO dispersed in 2-MeTHF.

and slow (> 10 ps) quenching processes occur during the decay of the 450 nm band species. The weak broad absorption band remained after 500 ps, which can be assigned to the excimer.

The TDR spectra were analyzed by applying a global fitting procedure to a set of decay curves including a three-component exponential and a constant. The reaction model applied to the excited state of Bp-PMO is shown in **Scheme 2**(a), where α and $(1-\alpha)$

are fractions of the S_1 state with faster (k_2) and slower (k_3) reaction rates, respectively. The time dependence of the excited species in Scheme 2 can be obtained under the initial condition of $FC(0) = FC_0$, $S_1(0) = 0$, and $E(0) = 0$ as follows:

$$FC(t)/FC_0 = \exp(-k_1 t), \tag{7}$$

$$\begin{aligned}
S_1(t)/FC_0 = -k_1 \{ &\alpha(k_1 - k_2)^{-1} \\
&+ (1-\alpha)(k_1 - k_3)^{-1} \} \exp(-k_1 t) \\
&+ \alpha k_1 (k_1 - k_2)^{-1} \exp(-k_2 t) \\
&+ (1-\alpha)k_1(k_1 - k_3)^{-1} \exp(-k_3 t),
\end{aligned} \tag{8}$$

$$\begin{aligned}
E(t)/FC_0 = k_1(k_1 - k_E)^{-1} \{ &\alpha k_2(k_1 - k_2)^{-1} \\
&+ (1-\alpha)k_3(k_1 - k_3)^{-1} \}\exp(-k_1 t) \\
&- \alpha k_1 k_2(k_1 - k_2)^{-1}(k_2 - k_E)^{-1}\exp(-k_2 t) \\
&- (1-\alpha)k_1 k_3(k_1 - k_3)^{-1}(k_3 - k_E)^{-1}\exp(-k_3 t) \\
&+ \{\alpha k_1 k_2(k_1 - k_E)^{-1}(k_2 - k_E)^{-1} \\
&+ (1-\alpha)k_1 k_3(k_1 - k_E)^{-1}(k_3 - k_E)^{-1}\}\exp(-k_E t).
\end{aligned} \tag{9}$$
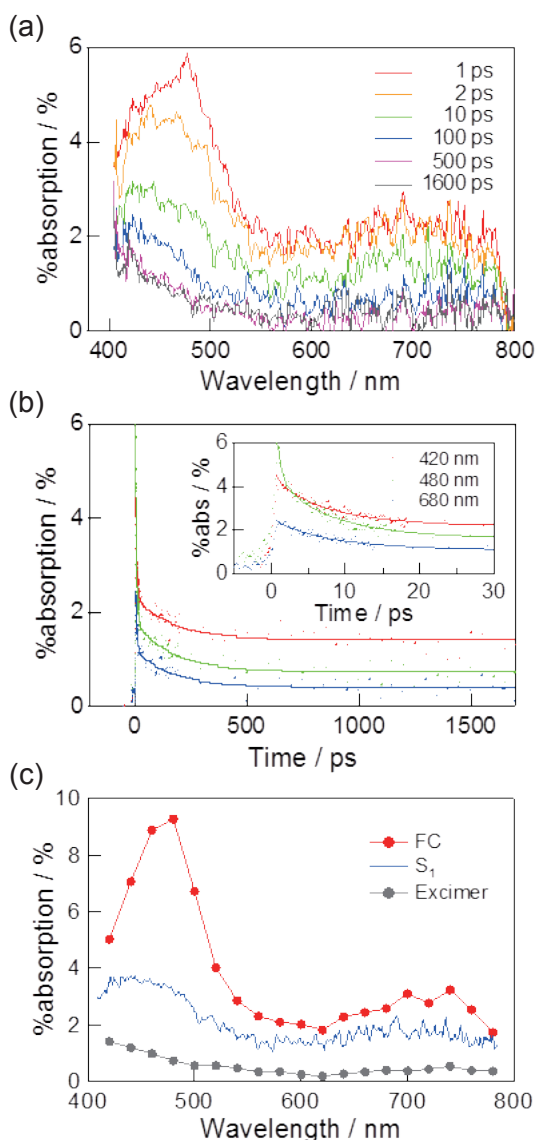
Fig. 5 (a) TDR spectra and (b) spectral time profiles for Bp-PMO powder after excitation at 266 nm at RT. The solid lines in (b) indicate simulated curves obtained using the global fitting program. (c) Reproduced absorption spectra for the FC, S_1, and excimer states of Bp-PMO.

M: Ground state of Bp in Bp-PMO, FC: FC state, S_1: Relaxed S_1 state, E: Excimer state
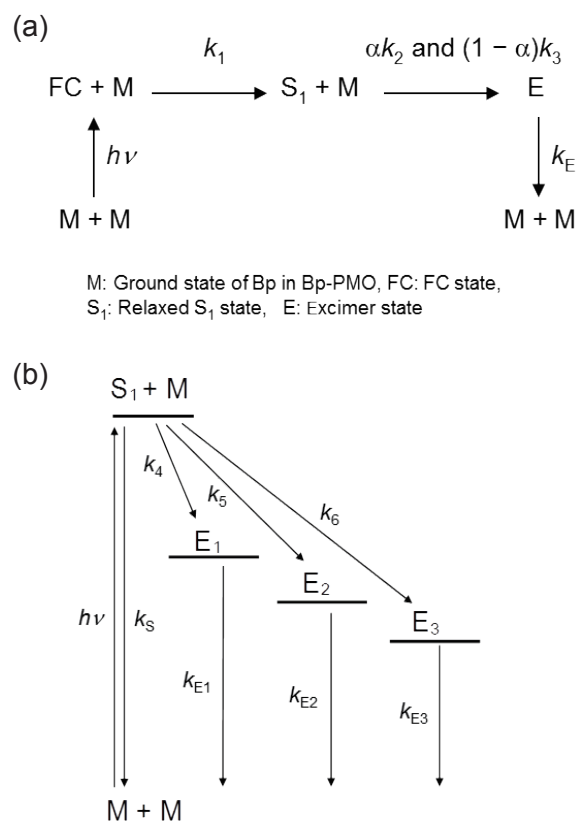
Scheme 2 Reaction model for Bp-PMO applied to (a) the TDR spectral analysis and (b) the analyses of the fluorescence rise and decay curves.

The observed transient absorption $\%abs(\lambda, t)$, at wavelength λ and time t, can be expressed by a superposition of Eqs. (7) to (9):

$$\%abs(\lambda, t) = A_6(\lambda)exp(- k_1 t), + A_7(\lambda)exp(- k_2 t) + A_8(\lambda)exp(- k_3 t) + A_9(\lambda), \tag{10}$$

where $A_6(\lambda)$, $A_7(\lambda)$, $A_8(\lambda)$, $A_9(\lambda)$ are fitting parameters. The $exp(- k_E t)$ term in Eq. (10) was assumed to be a time-independent constant $A_9(\lambda)$, because the decay of the E state was estimated as less than several % in the time scale of the TDR measurements. The fitting was applied to the set of time profiles by fixing $k_3^{-1} = 170$ ps determined by fluorescence decay analysis as described later. The values of k_1^{-1}, k_2^{-1}, and α were estimated to be 730 ± 95 fs, 7.0 ± 0.2 ps, and 0.64 ± 0.11, respectively. From these results, the absorption spectra of the FC and excimer states were reconstructed as $\%abs(\lambda, t)$ at $t = 0$ and the $A_9(\lambda)$ in Eq. (10), respectively. The absorption spectrum of the S_1 state was approximated from the mean spectrum of $\%abs(\lambda, t)$ from 2 to 10 ps. The $\%abs$ spectra of the FC, S_1, and excimer states are shown in Fig. 5(c).

The torsion angle of the two phenyl rings in Bp-PMO is discussed in relation to the spectral shape of the S_1 absorption. Mank et al. reported that the 680 nm band diminishes when the two phenyl rings of a biphenyl molecule cannot become planar in the S_1 state due to dimethyl substitution at the 2 and 2' positions.[39] Similarly, the relative intensity of the 680 nm band to that of the 450 nm band is largely decreased for Bp-PMO as compared to that for BTEBp in cyclohexane and for the neat liquid,[23] which suggests that the two phenyl rings of Bp in Bp-PMO are still distorted, even after relaxation to the S_1 state.

Figure 6(a) shows the time-resolved fluorescence spectra of Bp-PMO constructed from the rise and decay curves at RT. The fluorescence spectrum detected at 0-0.1 ns after laser irradiation shows an emission peak at 330 nm. The peak position was shifted to longer wavelength and the spectral band width was broadened during the observed time scale. Figure 6(b) shows fluorescence decay curves monitored at 320, 370, and 420 nm. The decay curves show multi-component exponential decay functions at every detected wavelength and a rise component was observed at 420 nm.

Thirty decay curves detected at different wavelengths were analyzed by applying the global fitting program.

At least four rate constants were required to obtain an acceptable fitting result, and thus, the reaction scheme indicated in Scheme 2(b) was used for the analytical model. The initial conditions applied at $t = 0$ were $S_1(0) = S_1^0$, $E_1(0) = E_1^0$, $E_2(0) = E_2^0$, and $E_3(0) = E_3^0$, because the time scale of the structural relaxation from the FC state to the S_1 state and the
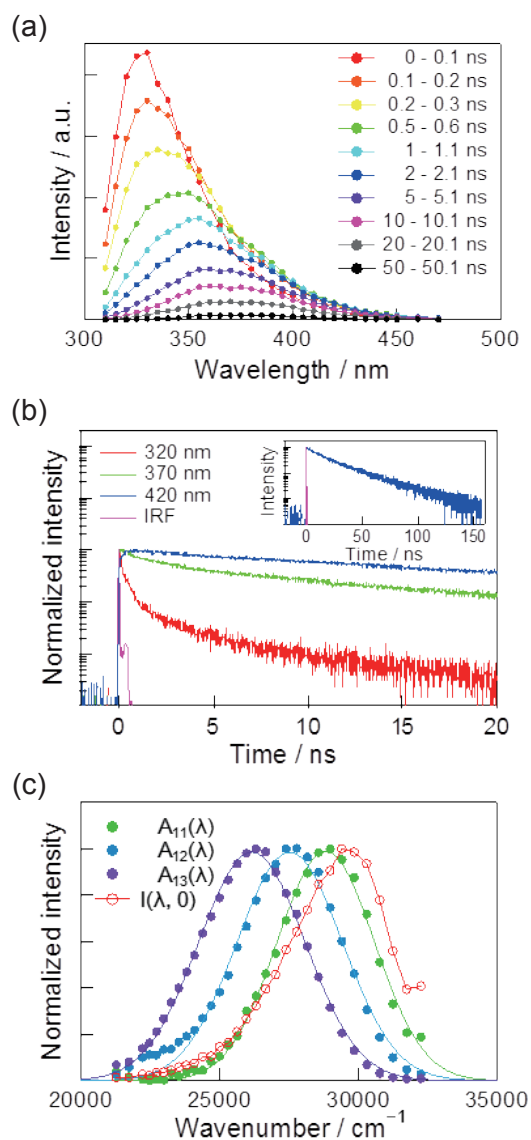
Fig. 6   (a) Time-resolved fluorescence spectra and (b) decay curves detected at 320, 370, and 420 nm at RT within 20 ps time scale for Bp-PMO powder. Inset: fluorescence time profile at 420 nm within a 160 ns time scale. (c) Reproduced spectra of $I(\lambda, 0)$, $A_{11}(\lambda)$, $A_{12}(\lambda)$, and $A_{13}(\lambda)$. Solid lines for $A_{11}(\lambda)$, $A_{12}(\lambda)$, and $A_{13}(\lambda)$ represent the fitting results using a Gaussian function.

rapid excimer formation (7.0 ps) from the S_1 state were much faster compared with IRF (*ca*. 30 ps). The solutions of the rate equations under the initial conditions are:

$$S_1(t) = S_1^0 \exp\{-(k_4 + k_5 + k_6 + k_S)t\}, \qquad (11)$$

$$
\begin{aligned}
E_1(t) = &-S_1^0 k_4 (k_4 + k_5 + k_6 + k_S - k_{E1})^{-1} \\
& \exp\{-(k_4 + k_5 + k_6 + k_S)t\} \\
& + \{S_1^0 k_4 (k_4 + k_5 + k_6 + k_S - k_{E1})^{-1} \\
& + E_1^0\}\exp(-k_{E1})t), \qquad (12)
\end{aligned}
$$

$$
\begin{aligned}
E_2(t) = &-S_1^0 k_5 (k_4 + k_5 + k_6 + k_S - k_{E2})^{-1} \\
& \exp\{-(k_4 + k_5 + k_6 + k_S)t\} \\
& + \{S_1^0 k_5 (k_4 + k_5 + k_6 + k_S - k_{E2})^{-1} \\
& + E_2^0\}\exp(-k_{E2})t), \qquad (13)
\end{aligned}
$$

$$
\begin{aligned}
E_3(t) = &-S_1^0 k_6 (k_4 + k_5 + k_6 + k_S - k_{E3})^{-1} \\
& \exp\{-(k_4 + k_5 + k_6 + k_S)t\} \\
& + \{S_1^0 k_6 (k_4 + k_5 + k_6 + k_S - k_{E3})^{-1} \\
& + E_3^0\}\exp(-k_{E3})t). \qquad (14)
\end{aligned}
$$

The observed fluorescence decay curves, $I(\lambda, t)$, can be obtained by summation of Eqs. (11) to (14):

$$
\begin{aligned}
I(\lambda, t) = &A_{10}(\lambda)\exp\{-(k_4 + k_5 + k_6 + k_S)t\} \\
& + A_{11}(\lambda)\exp(-k_{E3}t) + A_{12}(\lambda)\exp(-k_{E2}t) \\
& + A_{13}(\lambda)\exp(-k_{E3}t), \qquad (15)
\end{aligned}
$$

where $A_{10}(\lambda)$, $A_{11}(\lambda)$, $A_{12}(\lambda)$, and $A_{13}(\lambda)$ are fitting parameters. The results of the global fitting indicated time constants of $(k_4 + k_5 + k_6 + k_S)^{-1} = 170 \pm 47$ ps, $k_{E1}^{-1} = 1.3 \pm 0.2$ ns, $k_{E2}^{-1} = 8.2 \pm 0.7$ ns, $k_{E3}^{-1} = 27 \pm 2$ ns. Figure 6(c) shows the reproduced spectra of $I(\lambda, 0)$, $A_{11}(\lambda)$, $A_{12}(\lambda)$, and $A_{13}(\lambda)$. The spectral shape of $I(\lambda, 0)$ is close to that of $A_{11}(\lambda)$, except for a weak contribution of fluorescence from the S_1 state. This result implies that the observed fast S_1 decay process with a time constant of 7.0 ps is related mainly to the E_1 formation rather than the E_2 and E_3 formations, because the spectra of the pre-exponential factors ($A_{11}(\lambda)$, $A_{12}(\lambda)$, and $A_{13}(\lambda)$) indicate the fluorescence of the corresponding excimers with decay times of k_{E1}^{-1}, k_{E2}^{-1}, and k_{E3}^{-1}, respectively. The reproduced spectra of the excimers are Gaussian curves, as indicated by the solid line in Fig. 6(c), which supports the existence of least three types of excimer sites in Bp-PMO. Such excimer fluorescence bands with different peak positions, dependent on the intermolecular interactions, were reported for Bp units in a crystalline layered silicate, ilerite.[38]

The formation of multiple excimer sites could be attributed to the fluctuating packing structure of Bp in the PMO framework. It may be plausible that Bp with relatively short Bp-Bp distances is likely to rapidly form excimers (7.0 ps: E_1) with low activation energy, but such Bp would be well-condensed and thus have limited mobility for stabilization, which would result in high energy and short lifetime (1.3 ns) excimers. In contrast, Bp with relatively long Bp-Bp distances might form excimers slowly (170 ps for E_2 and E_3) with molecular motion for stabilization, which would result in low energy and long lifetime (8.2 ns for E_2 and 27 ns for E_3) excimers. The origin of the fluctuating packing structure is unclear at the present stage. However, it may result from flexibility of the silicate layer itself because the amount of residual silanol groups was found to have little influence on the spectral shape in steady-state fluorescence in Bp-silica hybrids with a similar molecular arrangement.

3. 3 Comparison of Ph-PMO and Bp-PMO

The reaction schemes for the excitation-relaxation process of Ph-PMO and Bp-PMO are summarized in **Scheme 3**. The Ph moieties of Ph-PMO exist as a monomer (no dimer and/or aggregate formation) in the ground state and form excimers in the excited state at RT, which is similar to Bp moieties of Bp-PMO. In contrast, the following differences in the excited state dynamics between the two PMOs are found:

(1) The excited state of Ph-PMO is delocalized between the Ph moieties and can migrate during its lifetime, while the excited state of Bp-PMO seems to be localized in one Bp moiety and remains there during its lifetime.

(2) Bp-PMO forms excimers at 77 K, while Ph-PMO does not.

(3) Three excimer states with different energies coexist in the excited state of Bp-PMO, whereas only one stable excimer was detected in Ph-PMO.

These differences may be explained by considering the intramolecular structural changes between the FC (twisted) and S_1 (planar) states of the Bp moiety for Bp-PMO. In the case of Ph-PMO, the delocalized FC state may relax to the stabilized exciton state without any large conformational changes. For Bp-PMO, in contrast, relaxation processes from the FC state to the

exciton state require concerted twisting motions in the neighboring Bp moieties, and this concerted low frequency intramolecular twisting can be disturbed easily by thermal fluctuations, resulting in the formation of the localized S_1 state of the Bp moiety. As a result, the localized S_1 state of the Bp moiety is considered to form the excimer with a smaller energy barrier compared to the case of the Ph moiety, which may be one of the reasons that Bp-PMO forms an excimer even at 77 K. In addition, the formation of excimers with different energies for Bp-PMO may be due to fluctuating arrangements of the Bp moieties in the flexible silica network. Meanwhile, in Ph-PMO, the exciton can migrate to the excimer forming site due to the larger activation barrier for the delocalization interaction.

4. Conclusion

This paper describes the excited-state dynamics of Ph moieties and Bp moieties in the framework of PMO powders. The differences between Ph-PMO and Bp-PMO were discussed based on the assumption that intramolecular structural changes of the Bp moiety by excitation were likely to hinder delocalization of its excited energy. The results clearly indicated that the differences in the excited state dynamics reflected the differences in the molecular level structures in the walls of the PMO.

Acknowledgements
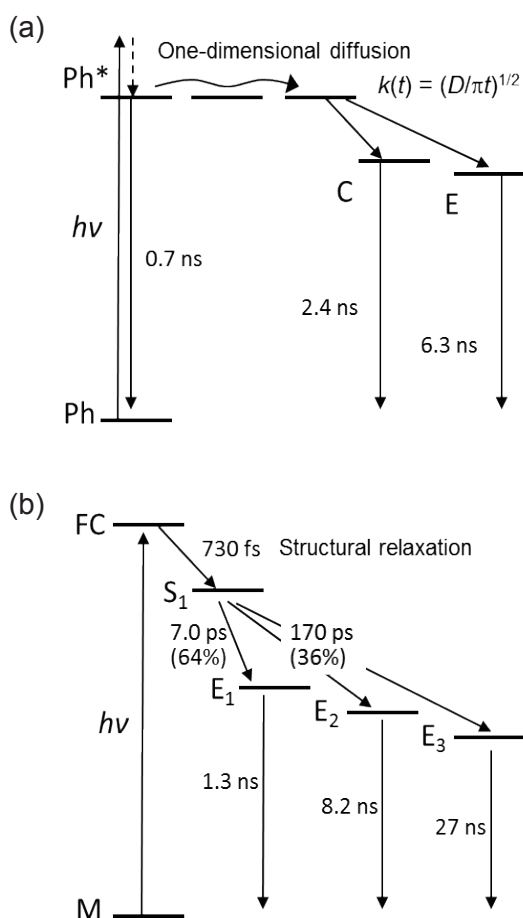
Scheme 3   Reaction scheme and lifetimes of excited states for (a) Ph-PMO and (b) Bp-PMO.

References

(1) Shea, K. J., Loy, D. A. and Webster, O., *J. Am. Chem. Soc.*, Vol. 114, No. 17 (1992), pp. 6700-6710.

(2) Loy, D. A. and Shea, K. J., *Chem. Rev.*, Vol. 95, No.5 (1995), pp. 1431-1442.

(3) Inagaki, S., Guan, S., Fukushima, Y., Ohsuna, T. and Terasaki, O., *J. Am. Chem. Soc.*, Vol. 121, No. 41 (1999), pp. 9611-9614.

(4) Melde, B. J., Holland, B. T., Blanford, C. F. and Stein, A., *Chem. Mater.*, Vol. 11, No. 11 (1999), pp. 3302-3308.

(5) Asefa, T., MacLachlan, M. J., Coombs, N. and Ozin, G. A., *Nature*, Vol. 402, No. 6764 (1999), pp. 867-871.

(6) Inagaki, S., Guan, S., Ohsuna, T. and Terasaki, O., *Nature*, Vol. 416, No. 6878 (2002), pp. 304-307.

(7) Kapoor, M. P., Yang, Q. and Inagaki, S., *J. Am. Chem. Soc.*, Vol. 124, No. 51 (2002), pp. 15176-15177.

(8) Sayari, A. and Wang, W., *J. Am. Chem. Soc.*, Vol. 127, No. 35 (2005), pp. 12194-12195.

(9) Cornelius, M., Hoffmann, F. and Fröba, M., *Chem. Mater.*, Vol. 17, No. 26 (2005), pp. 6674-6678.

(10) Mizoshita, N., Goto, Y., Kapoor, M. P., Shimada, T., Tani, T. and Inagaki, S., *Chem. - Eur. J.*, Vol. 15, No. 1 (2009), pp. 219-226.

(11) Goto, Y., Mizoshita, N., Ohtani, O., Okada, T., Shimada, T., Tani, T. and Inagaki, S., *Chem. Mater.*, Vol. 20, No. 13 (2008), pp. 4495-4498.

(12) Mizoshita, N., Goto, Y., Tani, T. and Inagaki, S., *Adv. Funct. Mater.*, Vol. 18, No. 22 (2008), pp. 3699-3705.

(13) Tani, T., Mizoshita, N. and Inagaki, S., *J. Mater. Chem.*, Vol. 19, No. 26 (2009), pp. 4451-4456.

(14) Mizoshita, N., Goto, Y., Tani, T. and Inagaki, S., *Adv. Mater.*, Vol. 21, No. 47 (2009), pp. 4798-4801.

(15) Mizoshita, N., Goto, Y., Maegawa, Y., Tani, T. and Inagaki, S., *Chem. Mater.*, Vol. 22, No. 8 (2010), pp. 2548-2554.

(16) Inagaki, S., Ohtani, O., Goto, Y., Okamoto, K., Ikai, M., Yamanaka, K., Tani, T. and Okada, T., *Angew. Chem., Int. Ed.*, Vol. 48, No. 22 (2009), pp. 4042-4046.

(17) Takeda, H., Goto, Y., Maegawa, Y., Ohsuna, T., Tani, T., Matsumoto, K., Shimada, T. and Inagaki, S., *Chem. Commun.*, Vol. 40 (2009), pp. 6032-6034.

(18) Maegawa, Y., Mizoshita, N., Tani, T. and Inagaki, S., *J. Mater. Chem.*, Vol. 20, No. 21 (2010), pp. 4399-4403.

(19) Takeda, H., Ohashi, M., Tani, T., Ishitani, O. and Inagaki, S., *Inorg. Chem.*, Vol. 49, No. 10 (2010), pp. 4554-4559.

(20) Ohashi, M., Aoki, M., Yamanaka, K., Nakajima, K., Ohsuna, T., Tani, T. and Inagaki, S., *Chem. - Eur. J.*, Vol. 15, No. 47 (2009), pp. 13041-13046.

(21) Mizoshita, N., Yamanaka, K., Shimada, T., Tani, T. and Inagaki, S., *Chem. Commun.*, Vol. 46, No. 48 (2010), pp. 9235-9237.

(22) Mizoshita, N., Ikai, M., Tani, T. and Inagaki, S., *J. Am. Chem. Soc.*, Vol. 131, No. 40 (2009), pp. 14225-14227.

(23) Yamanaka, K., Okada, T., Goto, Y., Tani, T. and Inagaki, S., *Phys. Chem. Chem. Phys.*, Vol. 12, No. 37 (2010), pp. 11688-11696.

(24) Okada, T., Yamanaka, K., Hirose, Y., Goto, Y., Tani, T. and Inagaki, S., *Phys. Chem. Chem. Phys.*, Vol. 13, No. 17 (2011), pp. 7961-7967.

(25) Yamanaka, K., Okada, T., Goto, Y., Ikai, M., Tani, T. and Inagaki, S., *J. Phys. Chem. C*, Vol. 117, No. 28 (2013), pp. 14865-14871.

(26) Yamanaka, K., Okada, T., Goto, Y., Tani, T. and Inagaki, S., *RSC Adv.*, Vol. 3, No. 34 (2013), pp. 14774-14779.

(27) Ishibashi, Y., Katayama, T., Saito, H., Yamanaka, K., Goto, Y., Tani, T., Okada, T., Inagaki, S. and Miyasaka, H., *J. Phys. Chem. C*, Vol. 118, No. 18 (2014), pp. 9419-9428.

(28) Yamanaka, K., Liu, X., Goto, Y. and Inagaki, S., *J. Phys. Chem. C*, Vol. 121, No. 27 (2017), pp. 14962-14967.

(29) O'Connor, D. V. and Phillips, D., *Time-correlated Single Photon Counting* (1984), pp. 158-210, Academic Press.

(30) Okada, T., Yamanaka, K., Goto, Y. and Inagaki, S., *Pol. J. Chem.*, Vol. 82, No. 4 (2008), pp. 729-739.

(31) Naqvi, K. R., Martins, J. and Melo, E., *J. Phys. Chem. B*, Vol. 104, No. 50 (2000), pp. 12035-12038.

(32) Nau, W. M. and Wang, X., *ChemPhysChem*, Vol. 3, No. 5 (2002), pp. 393-398.

(33) Carbonaro, C. M., Clemente, F., Corpino, R., Ricci, P. C. and Anedda, A., *J. Phys. Chem. B*, Vol. 109, No. 30 (2005), pp. 14441-14444.

(34) Anedda, A., Carbonaro, C. M., Clemente, F., Corpino, R. and Ricci, P. C., *J. Phys. Chem. B*, Vol. 109, No. 3 (2005), pp. 1239-1242.

(35) Bouvy, C., Marine, W., Sporken, R. and Su, B.-L., *Chem. Phys. Lett.*, Vol. 420, No. 1-3 (2006), pp. 225-229.

(36) Onida, B., Camarota, B., Ugliengo, P., Goto, Y., Inagaki, S. and Garrone, E., *J. Phys. Chem. B*, Vol. 109, No. 46 (2005), pp. 21732-21736.

(37) Sasaki, K., Nagasaka, M. and Kuroda, Y., *Chem. Commun.*, Vol. 24 (2001), pp. 2630-2631.

(38) Ishii, R., Ikeda, T., Itoh, T., Ebina, T., Yokoyama, T., Hanaoka, T. and Mizukami, F., *J. Mater. Chem.*, Vol. 16, No. 41 (2006), pp. 4035-4043.

(39) Mank, D., Raytchev, M., Amthor, S., Lambert, C. and Fiebig, T., *Chem. Phys. Lett.*, Vol. 376, No. 1-2 (2003), pp. 201-206.

Ken-ichi Yamanaka
  Research Fields:
    - Photochemistry
    - Physical Chemistry
    - Time-resolved Spectroscopy
  Academic Degree: Dr.Sci.
  Academic Societies:
    - The Chemical Society of Japan
    - The Japanese Photochemistry Association